Hindawi
Mathematical Problems in Engineering
Volume 2021, Article ID 8899995, 13 pages
https://doi.org/10.1155/2021/8899995

Research Article

Impact of Surface Undulation on Flow and Heat Transfer Characteristics in an Enclosure Filled with Nanoencapsulated Phase Change Materials (NEPCMs)

A. Alhashash [1] **and H. Saleh** [2]

[1]*Department of Mathematics, College of Science Jouf University, P.O. Box 2014, Sakaka, Saudi Arabia*
[2]*Mathematics Education Department, Universitas Islam Negeri Sultan Syarif Kasim, Pekanbaru 28293, Indonesia*

Correspondence should be addressed to H. Saleh; dr.habibissaleh@gmail.com

Received 29 September 2020; Revised 11 December 2020; Accepted 25 January 2021; Published 9 February 2021

Academic Editor: Mohamed Shaat

The present study investigates the natural convection in a wavy enclosure caused by a thermal difference between a cold wall and a hot undulated wall. The enclosure is filled with hybrid nanofluids. The hybrid nanofluids are formed of a phase change material (PCM) suspended in the water. The PCM utilizes polyurethane as the shell and nonadecane as the core. The core absorbs or releases its energy in the shape of latent heat inside the water and contributes to thermal energy storage and heat transfer. The governing equations are expressed in PDEs and solved by the finite element method (FEM). Parametric studies were used to analyze the solid concentration, fusion temperature, amplitude of corrugation, number of corrugations, and Rayleigh number. It is found that the heat transfer rate enhances by the rise of the latent heat of the NEPCM cores. The global heat transfer can be improved by more than 12% by adding 1% of NEPCM particles volume fraction. However, the heat transfer tends to decrease by applying the wavy surface.

1. Introduction

Nanotechnology deals with extremely small things that enable us to modify individual atoms. Choi [1] designed nanometer-sized materials, nanofluids, to increase the thermal conductivity of the fluids. Natural convection in enclosures filled with nanofluid was conducted by Khanafer et al. [2, 3], Hwang et al. [4], and Oztop and Abu-Nada [5, 6]. Öğüt [7] considered the dispersed argentum in the water, while Rashmi et al. [8] engineered the alumina-water nanofluids. Sheikhzadeh et al. [9] and Motlagh and Soltanipour [10] studied flow field and heat transfer in an enclosure where the transport mechanisms include Brownian and thermophoretic diffusions. Khanafer et al. [2] and Motlagh and Soltanipour [10] concluded that dispersing nanoparticles in host fluid would considerably improve the heat transfer.

Heat and mass transfer efficiency are important in many engineering devices. Surface waviness and nanofluids are two of the techniques with the goal of reducing the amount of energy required. The change of flow field with changes in wavy walls together with conductive fluid is a special feature that is not encountered in the conventional cooling system. Convection heat transfer in enclosures filled with nanofluids having wavy wall was studied by Abu-Nada and Oztop [11]. They concluded that the addition of alumina nanoparticles to the water increases the heat transfer rate. Esmaeilpour and Abdollahzadeh [12] studied natural convection and entropy generation of copper-water inside an enclosure having different types of vertical wavy walls. Nikfar and Mahmoodi [13] exhibited that considerable differences occur between the rates of heat transfer in the wavy enclosure for the two viscosity models of the nanofluids. Mansour and Bakier [14] indicated that the heat transfer rate can be optimized by adjusting the surface waviness together with the Rayleigh number and nanoparticle concentration. The analysis considering three different nanofluids was investigated by Cho

et al. [15] and later Cho [16] considered wavy enclosure with partial heating. Enhancement of the heat transfer rate of a wavy surface by employing hybrid nanofluid was obtained by Takabi and Salehi [17]. Sheikholeslami et al. [18] included the magnetic parameter with different orientations of the wavy enclosure. Sheikholeslami and Ellahi [19] studied the hydrothermal treatment utilizing electrohydrodynamic nanofluid in an enclosure with a corrugated upper wall. The convection enhancement of nanofluid with double wavy walls having different phase deviations was investigated by Tang et al. [20]. Shirvan et al. [21] applied a cosine corrugated surface and Sheremet et al. [22] applied a nonuniform heating. An open wavy cavity filled hybrid nanofluid was considered by Ashorynejad and Shahriari [23]. Hashim et al. [24] observed that heat transfer inside the wavy enclosure is enhanced by introducing alumina and choosing the optimal number of undulations. Dogonchi et al. [25] applied CVFEM to predict magnetohydrodynamic convective flow of copper-water in the wavy enclosure. Dogonchi et al. [26] considered the impact of different shapes of nanoparticles in a locally heated complex wavy enclosure. They concluded that the particle shape parameter plays a crucial role in the heat performance.

Solidification of nanoenhanced phase change material (PCM) in a wavy enclosure was considered by Kashani et al. [27]. A horizontal heated square cavity filled with nanoenhanced PCM for the flat surface was initially started by Sebti et al. [28]. Then, Ho and Gao [29] experimentally studied this configuration. Later, Tasnim et al. [30] studied the convection influence on the melting process of the new type of PCM inside the porous enclosure. Abdollahzadeh and Esmaeilpour [31] proposed phase change material having nanofluids and corrugate surface. They concluded that the increasing effects of heat transfer on solidification are due to distortion on the surface. Dhaidan [32] considered several types of enclosures such as rectangular, spherical, cylindrical, and annular. They found that the nanostructures assist the heat transfer rate. Ghalambaz et al. [33] demonstrated that the hybrid nanoparticles enhance the fusion performance of nanoenhanced PCM in a square enclosure. Al-Jethelah et al. [34] compared melting processes between pure PCM and nano-PCM. Selimefendigil et al. [35] studied the conjugate heat transfer characteristic of nanofluid in a square enclosure, where a PCM is attached on the vertical wall. Bondareva et al. [36] reported that nano-PCM melts earlier for the tilted angle greater than 90° at the Rayleigh number.

The latest nanotechnology product is nanoencapsulated phase change materials (NEPCMs). This new material separates a shell as a capsule and a core inside. The core is PCM with a specific fusion temperature. It enables absorbing or releasing large energy from the latent heat [37]. Fang et al. [38] proposed the NEPCMs composed in situ polymerization techniques. They utilized the n-tetradecanes as the core and urea and formaldehyde for the cover. Sodium dodecyl sulfate was utilized as the emulsifier and resorcin was utilized as the system modifier. Jamekhorshid et al. [39] reviewed the methods utilized in the microencapsulated phase change materials (MEPCMs). Shchukina et al. [40] summarized some techniques used for the encapsulation phase change materials for the new design of energy storage device. Nazir et al. [41] proposed new ideas in enhancing the thermal energy storage that applies the PCMs through encapsulation. Recently, Ghalambaz et al. [42] and Hajjar et al. [43] investigated the enhancement heat transfer of NEPCMs in an enclosure having a flat surface.

The present study aims to study the natural convection in a wavy enclosure filled with water containing nanoencapsulated phase change material. The main parameters in this simulation are Rayleigh number, solid volume fraction, fusion temperature, amplitude, and number of corrugations. The natural convection problem of NEPCMs in an enclosure with corrugated surface could be applied to the solar heating heat exchangers. Here, the corrugated absorber improves the exergetic performance and the NEPCMs increase the thermal performance.

2. Model Formulation

A schematic model under consideration is illustrated in Figure 1. The enclosure has a size L. The right wall has a cold temperature T_c, while the left corrugated wall has a hot temperature T_h. Other walls are assumed to be insulated. The function of the left and the right wavy surfaces is

$$f(y) = A\cos(2N\pi y), \tag{1}$$

where A and N are amplitude and number of corrugations, respectively.

The NEPCMs are made of phase change materials. This advanced material contains an outer shell and a core inside. The outer shell is polyurethane and the core is nonadecane. The thermophysical properties of the applied materials are tabulated in Table 1. The inner subjects to a phase change to fluid in the fusion temperature interval with $T_h < T_f < T_c$. The phase change temperature and the latent heat of the inner core are 305 (K) and 211 (kJ/kg), respectively. Specifically, the PCM core of the hybrid nanoparticles can absorb/release a notable amount of energy in the form of latent heat. Moreover, the latent heat of the nanoparticle cores can contribute to energy transport inside the base fluid. The Boussinesq approximation is applied for the density variation. The suspension of NEPCMs and hot fluid is assumed to be uniform and stable. Based on these considerations, the continuity, momentum, and heat transfer equations can be written as follows [42, 43]:

$$\begin{aligned} \nabla \cdot \mathbf{v} &= 0, \\ \rho_b \cdot \nabla \mathbf{v} &= -\nabla p + \nabla \cdot \left(\mu_b \nabla \mathbf{v}\right) + (\rho\beta)_b g\left(T - T_c\right), \\ \left(\rho C_p\right)_b \mathbf{v} \cdot \nabla T &= -\nabla \cdot \left(k_b \nabla T\right), \end{aligned} \tag{2}$$

where subscript b refers to the bulk properties of the hybrid nanofluid, g is the acceleration due to gravity, and ρ_b, k_b, and β_b are the density, thermal conductivity, and thermal expansion coefficient of the base liquid at room temperature, respectively.

The density of the mixture is written as a weighted relation of the water and NEPCM dispersed particles [45]:

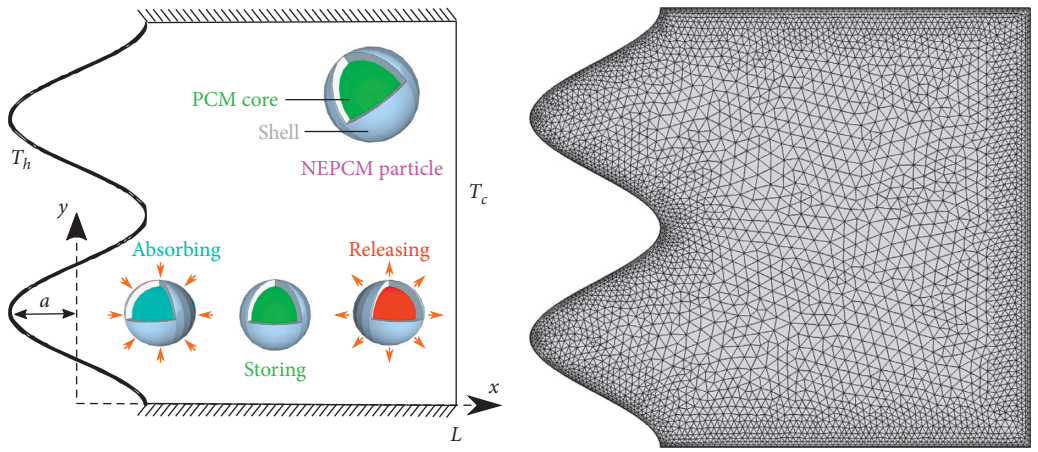

Figure 1: (a) Schematic representation of the wavy enclosure having NEPCM nanofluids. (b) Mesh distribution.

Table 1: The thermophysical properties of the applied materials [44].

Materials	ρ (kg/m^3)	μ (N s/m^2)	k (W m^{-1}K^{-1})	C_p (J/kg K)	β (1/K)
Water	997.1	0.00089	0.613	4.1790	0.00021
Polyurethane	786	–	–	1.3177	0.0001728
Nonadecane	721	–	–	2.0370	–

$$\rho_b = (1-\phi)\rho_f + \phi\rho_p. \tag{3}$$

The symbols p and f denote NEPCM particles and the water, respectively.

The density of NEPCM particles is defined as follows:

$$\rho_p = \frac{(1+\iota)\rho_{\text{co}}\rho_{\text{sh}}}{\rho_{\text{sh}} + \iota\rho_{\text{co}}}, \tag{4}$$

where ρ_{sh} is density of the shell, while ρ_{co} is density of the core. ι is the core-shell mass ratio: $\iota \sim 0.447$ [44]. Furthermore, the density of the core is the mean of the fluid and solid phases of the phase change material. The specific heat capacitance of the suspension can be evaluated as

$$C_{p,b} = \frac{(1-\phi)\left(\rho C_p\right)_f + \phi\left(\rho C_p\right)_p}{\rho_p}. \tag{5}$$

The specific heat capacitance subject to no phase change, $C_{p,p}$, is evaluated by the following function:

$$C_{p,p} = \frac{\left(C_{p,\text{co}} + \iota C_{p,\text{sh}}\right)\rho_{\text{co}}\rho_{\text{sh}}}{(\rho_{\text{sh}} + \iota\rho_{\text{co}})\rho_p}. \tag{6}$$

It is noted that the heat capacity of the core is the mean of the heat capacities of the fluid and solid states. This is due to the nanoparticles core subject to solid and fluid phase; then the latent heat was engaged in the heat capacity of the NEPCM. This heat can be formulated by performing rectangular, triangular, or sinusoidal functions as follows [46]:

$$\begin{aligned}
C_{p,p} &= C_{p,\text{co}} + \frac{h_{sf}}{T_{Mr}},\\
C_{p,p} &= C_{p,\text{co}} + \left\{\frac{\pi}{2}\cdot\left(\frac{h_{sf}}{T_{Mr}} - C_{p,\text{co}}\right)\cdot\sin\left(\pi\frac{T - T_{\text{fu}} + (T_{Mr}/2)}{T_{Mr}}\right)\right\},\\
C_{p,p} &= C_{p,\text{co}} + 2\left(\frac{h_{fs}}{T_{Mr}^2} - \frac{C_{p,\text{co}}}{T_{Mr}}\right)\left(T - T_{fu} + \frac{T_{Mr}}{2}\right),
\end{aligned} \tag{7}$$

where T_{Mr} is the temperature range. This range prevents the discontinuity in energy balance. The overall heat capacity of the NEPCM core including the sensible and fusion temperature is evaluated based on T_{Mr}:

$$C_{p,p} = C_{p,\text{co}} + \left\{\frac{\pi}{2}\cdot\left(\frac{h_{sf}}{T_{Mr}} - C_{p,\text{co}}\right)\cdot\sin\left(\pi\frac{T - T_{fu} + (T_{Mr}/2)}{T_{Mr}}\right)\right\}\gamma, \tag{8}$$

where

$$\gamma = \begin{cases} 0, & T < T_{fu} - \dfrac{T_{Mr}}{2},\\ 1, & T_{fu} - \dfrac{T_{Mr}}{2} < T < T_{fu} + \dfrac{T_{Mr}}{2},\\ 0, & T > T_{fu} + \dfrac{T_{Mr}}{2}, \end{cases} \tag{9}$$

and the thermal volume expansion coefficient of the suspension is written as

$$\beta_b = (1-\phi)\beta_f + \phi\beta_p. \tag{10}$$

The functions shown below are performed to calculate the thermal conductivity of suspension consisting of nanoencapsulated particles [42]:

$$\frac{k_b}{k_f} = 1 + Nc\phi. \tag{11}$$

The dynamic conductivity of suspension is

$$\frac{\mu_b}{\mu_f} = 1 + Nv\phi, \tag{12}$$

where Nc and Nv in the above equations refer to the numbers of thermal conductivity and viscosity, respectively. The larger the values of numbers of thermal conductivity and viscosity, the larger the increase in the thermal conductivity and dynamic viscosity of the suspension. These values are constant. Ghalambaz et al. [42] evaluated these values for some nanofluids and hybrid nanofluids. It is noted that these functions are valid only for nanofluids suspension when $\phi < 0.05$.

Dimensionless quantities were used as follows:

$$\begin{aligned}
X &= \frac{x}{L},\\
Y &= \frac{y}{L},\\
\delta &= \frac{\delta^*}{L},\\
U &= \frac{uL}{\alpha_f},\\
V &= \frac{vL}{\alpha_f},\\
P &= \frac{p\ell^2}{\rho_f \alpha_f^2},\\
\Theta &= \frac{T - T_c}{T_h - T_c}.
\end{aligned} \tag{13}$$

The nondimensional mathematical formulations become

$$\begin{aligned}
&\frac{\partial U}{\partial X} + \frac{\partial V}{\partial Y} = 0,\\
&\left(\frac{\rho_b}{\rho_f}\right)\left(U\frac{\partial U}{\partial X} + V\frac{\partial U}{\partial Y}\right) = -\frac{\partial P}{\partial X} + \Pr\left(\frac{\mu_b}{\mu_f}\right)\left(\frac{\partial^2 U}{\partial X^2} + \frac{\partial^2 U}{\partial Y^2}\right),\\
&\left(\frac{\rho_b}{\rho_f}\right)\left(U\frac{\partial V}{\partial X} + V\frac{\partial V}{\partial Y}\right) = -\frac{\partial P}{\partial Y} + \Pr\left(\frac{\mu_b}{\mu_f}\right)\left(\frac{\partial^2 V}{\partial X^2} + \frac{\partial^2 V}{\partial Y^2}\right)\\
&\qquad + \mathrm{RaPr}\frac{(\rho\beta)_b}{(\rho\beta)_f}\Theta,\\
&Cr\left(U\frac{\partial \Theta}{\partial X} + V\frac{\partial \Theta}{\partial Y}\right) = \frac{k_b}{k_f}\left(\frac{\partial^2 \Theta}{\partial X^2} + \frac{\partial^2 \Theta}{\partial Y^2}\right).
\end{aligned} \tag{14}$$

The dimensionless boundary conditions are

$$\begin{aligned}
&U = V = 0,\\
&\frac{\partial \Theta}{\partial Y} = 0 \text{ on bottom and top walls},\\
&U = V = 0,\\
&\Theta = 1 \text{ on left wavy wall},\\
&U = V = 0,\\
&\Theta = 0 \text{ on right wavy wall},
\end{aligned} \tag{15}$$

and the Rayleigh number, Ra, and Prandtl number, Pr, are nondimensional quantities defined as

$$\begin{aligned}
\mathrm{Ra} &= \frac{g\rho_f \beta_f \Delta T \ell^3}{\alpha_f \mu_f},\\
\mathrm{Pr} &= \frac{\mu_f}{\rho_f \alpha_f}.
\end{aligned} \tag{16}$$

Also,

$$\begin{aligned}
\left(\frac{\rho_b}{\rho_f}\right) &= (1-\phi) + \phi\left(\frac{\rho_p}{\rho_f}\right),\\
\left(\frac{\beta_b}{\beta_f}\right) &= (1-\phi) + \phi\left(\frac{\beta_p}{\beta_f}\right).
\end{aligned} \tag{17}$$

It is considered that the thermal expansion of the NEPCMs is equal to the water and, therefore, $(\beta_b/\beta_f) \sim 1$. Cr is the heat capacity of the mixture over the sensible heat capacity of the water:

$$Cr = \frac{(\rho C_p)_b}{(\rho C_p)_f} = (1-\phi) + \phi\lambda + \frac{\phi}{\delta \mathrm{Ste}} f, \tag{18}$$

where the sensible heat capacity ratio λ, the melting range ε, and Stefan number Ste can be stated as follows:

$$\begin{aligned}
\lambda &= \frac{\left(C_{p,\mathrm{co}} + \iota C_{p,\mathrm{sh}}\right)\rho_{\mathrm{co}}\rho_{\mathrm{sh}}}{(\rho C_p)_f(\rho_{\mathrm{sh}} + \iota\rho_{\mathrm{co}})},\\
\varepsilon &= \frac{T_{Mr}}{\Delta T},\\
\mathrm{Ste} &= \frac{(\rho C_p)_f \Delta T(\rho_{\mathrm{sh}} + \iota\rho_{\mathrm{co}})}{\alpha_f\left(h_{sf}\rho_{\mathrm{co}}\rho_{\mathrm{sh}}\right)}.
\end{aligned} \tag{19}$$

As extra information, the dimensionless fusion relation, f, is stated as

$$f = \frac{\pi}{2}\sin\left(\frac{\pi}{\varepsilon}\left(\Theta - \Theta_{\mathrm{fu}} + \frac{\varepsilon}{2}\right)\right)\sigma, \tag{20}$$

where

$$\sigma = \begin{cases} 0, & \Theta < \Theta_{\text{fu}} - \dfrac{\varepsilon}{2}, \\ 1, & \Theta_{\text{fu}} - \dfrac{\varepsilon}{2} < \Theta < \Theta_{\text{fu}} + \dfrac{\varepsilon}{2}, \\ 0, & \Theta > \Theta_{\text{fu}} + \dfrac{\varepsilon}{2}. \end{cases} \quad (21)$$

Here, Θ_{fu}, the nondimensional fusion temperature, is

$$\Theta_{\text{fu}} = \frac{T_{\text{fu}} - T_c}{\varepsilon T}. \quad (22)$$

The local Nusselt number calculated at the hot wall is

$$\text{Nu} = -\frac{1 + Nc\phi}{2} \frac{\partial \Theta}{\partial n}. \quad (23)$$

Finally, the averaged Nusselt number at the hot surface is calculated as

$$\overline{\text{Nu}} = \frac{1}{W} \int_0^1 \text{Nu}\, \text{d}n, \quad (24)$$

where W is the length of corrugated wall.

3. Computational Methodology

The governing dimensionless equations in the form of PDEs are solved numerically by using Galerkin finite element approach to determine the convective flows distribution inside the wavy cavity. The mathematical model is established in strong formulation; then weak formulations of the model are obtained by multiplying the equations by a test function and integrating the modified equations over the domain.

The principle of FEM is dividing the domain into subdomains. The solution element of the mathematical calculation is generated by a triangular mesh. The triangular mesh arrangements calibrate specifically for fluid dynamics problems. The Galerkin FEM uses the same function for both the test and basis functions. The integral equations can be solved using Galerkin weighted residual technique. The residual integrations of the continuity, momentum, and heat transfer equations in X and Y directions are employed by using Gauss's method. A Newton method is used to solve the system nonlinear equations in the matrix form. The iteration approach is adapted through PDEs solver COMSOL. The iteration is considered to be a convergence solution when the corresponding error of velocities and temperatures is equal to or less than 10^{-6}.

To achieve the optimal grid size, the grid independency test is conducted to make definite the variables independent from the grid calibration. Grid configurations are coarser, coarse, normal, fine, finer, extra fine, and extremely fine and are employed as shown in Table 2. The numerical results are observed to be free from variation by increasing the number of elements. Considering both time calculation and the error, an extra fine was selected for all the computations done in this paper. As a verification, current works (left) of streamlines are validated with that obtained by Adjlout et al. [47] (right) for the sinusoidal wavy wall at $\text{Ra} = 10^5$, $A = 0.05$, and $N = 1, 3$ without NEPCM as shown in Figure 2.

Table 2: Grid sensitivity checks for the average Nusselt number and the maximum value of stream function at $\text{Ra} = 10^7$, $A = 0.1$, $N = 4$, and $\varphi = 0.03$.

Predefined Mesh size	Domain Elements	Boundary Elements	$\overline{\text{Nu}}$	$\lvert\Psi\rvert_{\max}$	CPU Time (s)
Coarser	3593	283	13.844	7.895	17
Coarse	4874	342	13.838	7.487	21
Normal	5995	369	13.872	7.341	21
Fine	8280	420	13.895	7.3162	25
Finer	13466	608	13.855	7.192	36
Extra fine	29372	1042	13.855	7.123	78
Extremely fine	36480	1042	13.854	7.114	100

Additional validation is performed by comparison with the published work of Ghalambaz et al. [42], which is natural convection of NEPCMs in an enclosure having flat surface at $\phi = 0.05$, $\theta_f = 0.3$, $\text{Ste} = 0.313$, and $\text{Ra} = 10^5$ as shown in Figure 3. The comparison reveals good agreement with the reported studies. These comprehensive verification efforts demonstrated the robustness and accuracy of the present computation.

4. Results and Discussion

Parametric studies were used to analyze the related nondimensional quantity: the amplitude of undulated surface, $0 \le A \le 0.3$, the number of undulated surface, $3 \le N \le 6$, the fusion temperatures, $0.1 \le \theta_f \le 0.5$, the Rayleigh number, $10^0 \le \text{Ra} \le 10^6$, and nanoparticles concentration, $0.0 \le \phi \le 0.05$. The core weight of the nanoparticles is below water, and their shell weight is above water, so that the density ratio is below unity. The thermal expansion coefficient water is greatly above these particles. The dilute solution of NEPCMs has $Nc = 23.8$ and $N\nu = 12.5$ [44]. The sensible capacity ratio of the NEPCM is 0.32.

Figure 4 shows the development of the streamlines, isotherms, and heat capacity ratio distribution inside the wavy enclosure filled with 5% NEPCM for various numbers of corrugations N at $\theta_f = 0.1$, $\text{Ste} = 0.2$, $A = 0.3$, and $\text{Ra} = 10^6$. The strength of the flow movement enhances by increasing the wavy frequency. The formation of eye vortices is also modified by calibrating the shape of undulated wall. The isotherms are almost unchanging by varying the undulated number. It is noted that the fluid volumes for all enclosures are equal.

Figure 5 exhibits the development of the streamlines, isotherms, and heat capacity ratio distribution by increasing the fusion temperatures at $\text{Ra} = 10^6$, $\phi = 0.05$, $\text{Ste} = 0.2$, $A = 0.3$, and $N = 4$. Varying the fusion temperatures inconsiderably affects the streamlines and isotherms. The distribution of temperature at the boundary was not changed by varying θ_f. At $\theta_f = 0.1, 0.5$, the double eyes of vortex appear in the core. The heat capacity ratio exhibits a ribbon-form area near the fixed temperature line of fusion. The blue area displayed in the Cr contours refers to the area

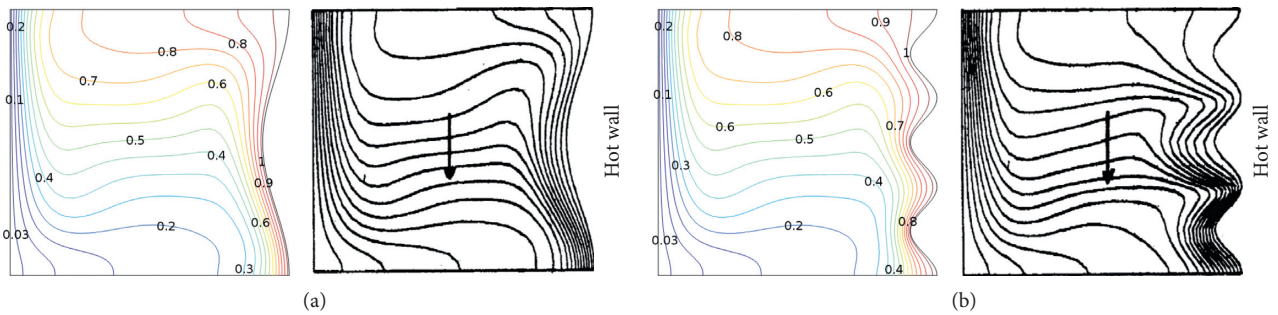

Figure 2: Validation of present streamlines with that obtained by Adjlout et al. [47] for the sinusoidal wavy wall at Ra = 10^5, $A = 0.05$, and $N = 1, 3$ without NEPCM.

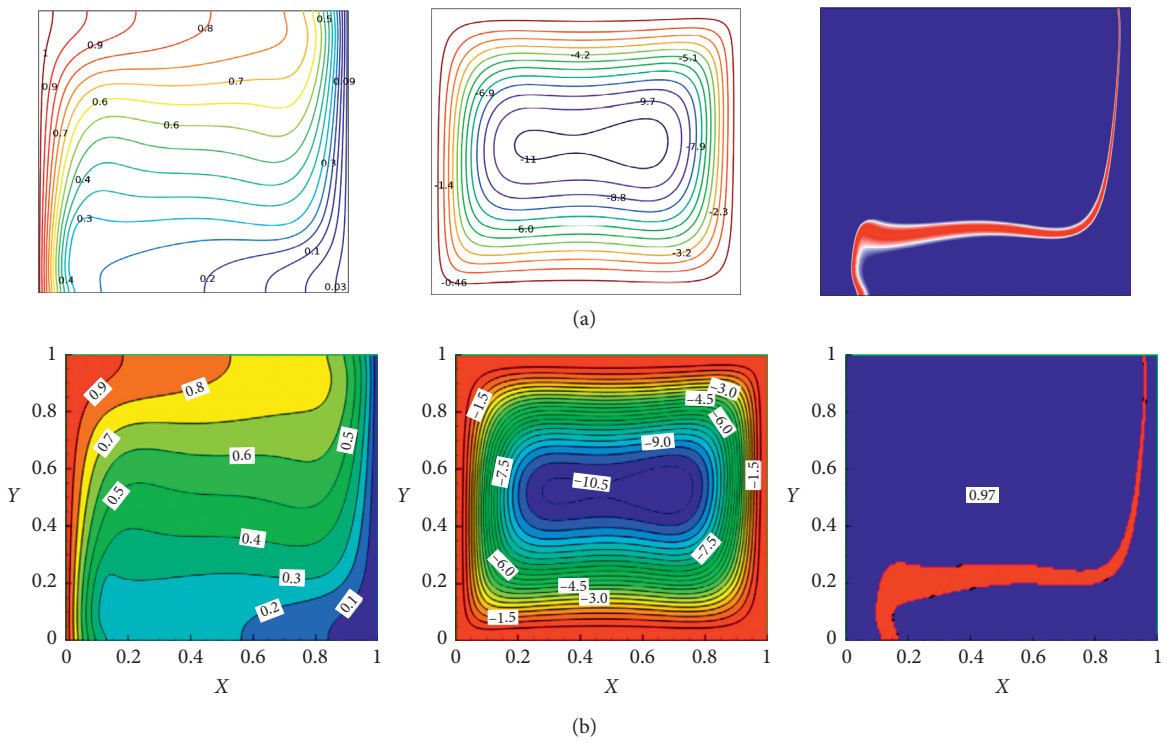

Figure 3: Comparison of calculated streamlines and isotherms of the present paper (left) with those of Ghalambaz et al. [42] (right) for the natural convection of NEPCMs in an enclosure having flat surface at $Nc = Nv = 3.0$, $\phi = 0.05$, $\theta_f = 0.3$, Ste = 0.313, and Ra = 10^5.

of phase change. The ribbon form of the melting area is extremely thin adjacent to the right of the top wall. This observation justifies why the large temperature gradients were revealed at these regions. The blue area gets larger when the fusion temperatures get higher. When the fusion temperature approximates the hot or cold surfaces temperature, the heat transfer improvement because of the phase change is low. The melting zone moves to the right when the fusion temperature increases. This mechanism indicates that a large amount of the NEPCMs releases the latent heat and solidifies.

Figure 6 shows the evolution of the streamlines, isotherms, and heat capacity ratio distribution by increasing the Rayleigh number at $\phi = 0.05$, $\theta_f = 0.1$, $A = 0.3$, and $N = 4$. At a small Rayleigh number, the flows movement is weak; meanwhile, at a larger Rayleigh number, the flows movement is strong and denser thermal layer close to the right surface is formed. This happens because the high Rayleigh numbers extend heating intensity, more particles are spread out inside recirculating zones, and, consequently, more deposition occurs in the lower zone of the enclosure. Phase change of the inner core happens when the temperature reaches the fusion temperature. This conveys that adjusting the heating intensity would modify the area of the phase change in terms of directions, locations, and area. This result is supported by the appearance of the heat capacity ratio, where the blue-ribbon-shaped area refers to the melting and solidification region. The area of phase change gets larger when the Rayleigh number gets stronger.

Figure 7 shows a connection between the average Nusselt number, $\overline{\mathrm{Nu}}$, and the Rayleigh number, Ra, at $\phi = 0.05$, $\theta_f = 0.1$, Ste = 0.2, and $A = 0.3$. Heat transfer rate decreases

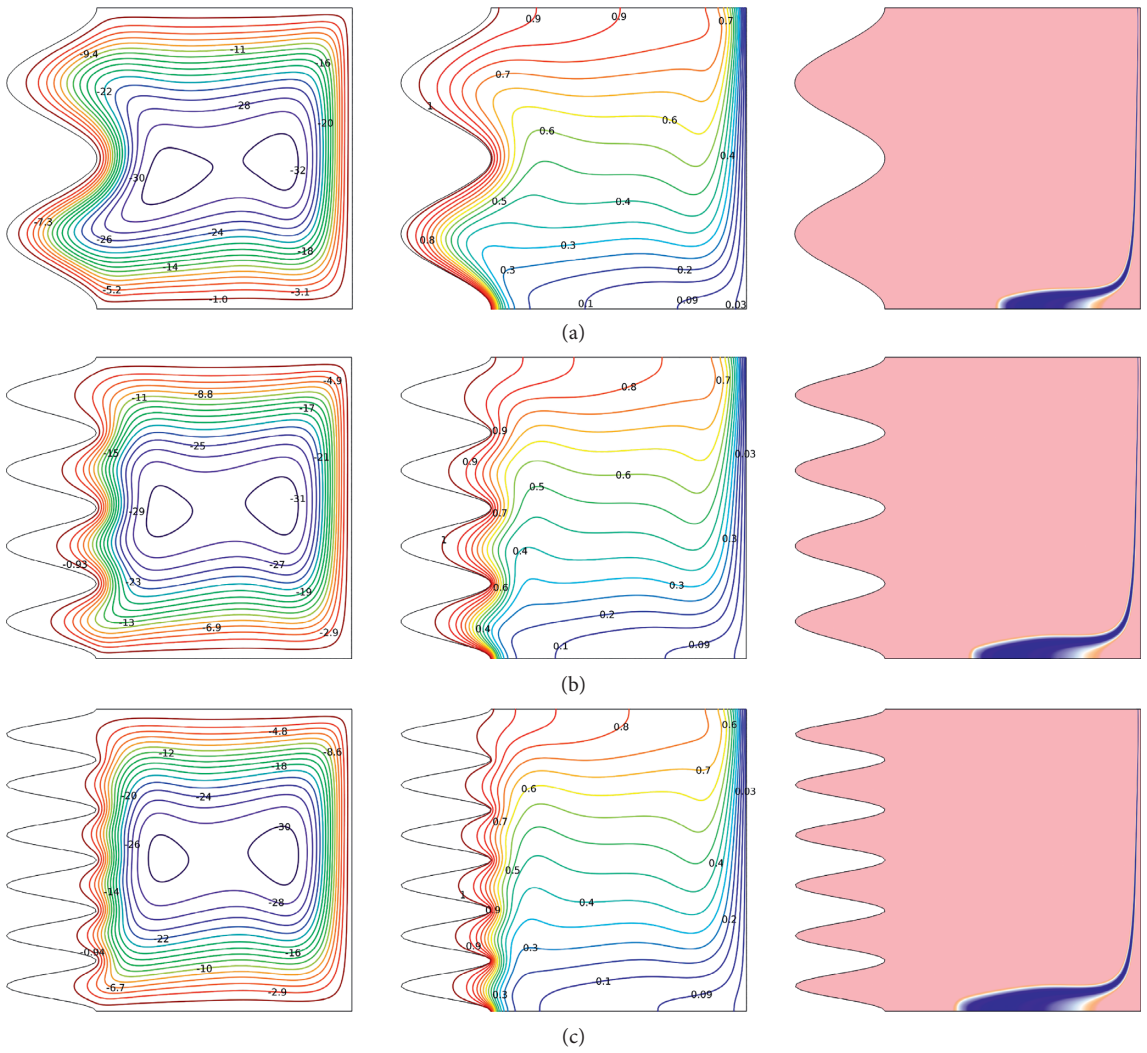

Figure 4: Development of the streamlines, isotherms, and heat capacity ratio for various numbers of corrugations N at $\phi = 0.05$, $\theta_f = 0.1$, Ste = 0.2, $A = 0.3$, and Ra = 10^6. (a) $N = 2$. (b) $N = 4$. (c) $N = 6$.

with increasing the undulation number. The reduction is more pronounced at a high Rayleigh number, Ra. This fact is due to the fact that the high convective flow covering almost the entire wavy cavity induces a sharply thermal gradient near the wavy boundary but, at the same time, the surface volume area increases so that the Nu ratio is reduced. The effect of waviness frequency on heat transfer becomes negligible for low heating intensity. Details relationship of Nusselt number against undulation amplitude for a small and a high gravitational force will be illustrated as follows.

Figure 8 exhibits a connection between the average Nusselt number, $\overline{\mathrm{Nu}}$, and the Rayleigh number, Ra, at $\phi = 0.05$, $\theta_f = 0.1$, and $N = 4$. Heat transfer performance is slightly modified by adjusting the undulation amplitude. The corrugated properties of the flow have insignificant effect because of the plain nature of the flow and the presence of eye convective currents in the center of the wavy cavity.

Figure 9 exhibits a relationship between the average Nusselt number, $\overline{\mathrm{Nu}}$, and the Rayleigh number, Ra, at $\phi = 0.05$, $A = 0.3$, Ste = 0.2, and $N = 4$. Heat transfer performance increases with increasing the fusion temperature. The fusion temperature is the change in its enthalpy resulting from providing heat to a specific quantity of the NEPCM to alter its properties from a solid to a liquid at constant pressure. The average Nusselt number is unchanged by increasing latent heat from 0.3 to 0.5. Effect of low or high heat of fusion on heat transfer becomes negligible for small Rayleigh number. The results in this figure confirm that the optimum fusion temperature of the NEPCM significantly depends on the heating intensity.

Figure 10 exhibits a relationship between the average Nusselt number, $\overline{\mathrm{Nu}}$, and the fusion temperature, θ_f, for the values of Stefan number at $\phi = 0.05$, $A = 0.3$, Ra = 10^5, and $N = 4$. The heat transfer increases by decreasing the Stefan number. This is due to the fact that when the latent heat of the nonadecane increases, the Stefan number reduces. Reducing the Stefan number brings about an increase in the nonadecane latent heat, which enhances the convective flow. The Nusselt number profiles are symmetric about line $\theta_f = 0.5$. The heat transfer enhances by increasing the fusion

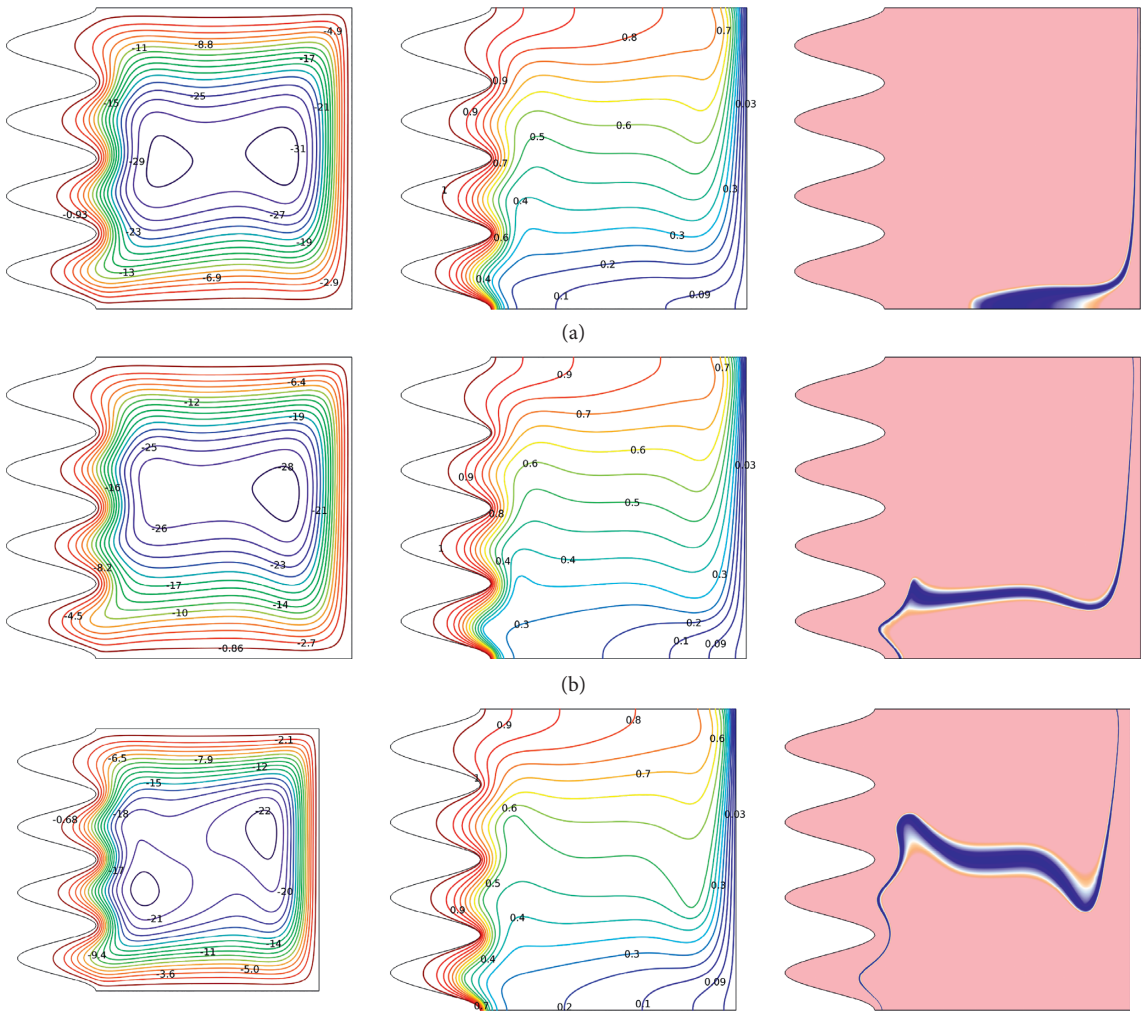

(a) (b) (c)

Figure 5: Influences of the fusion temperature on streamlines (left), isotherms (middle), and heat capacity ratio distribution (right) at Ra = 10^6, $\phi = 0.05$, Ste = 0.2, $A = 0.3$, and $N = 4$. (a) $\theta_f = 0.1$. (b) $\theta_f = 0.3$. (c) $\theta_f = 0.5$.

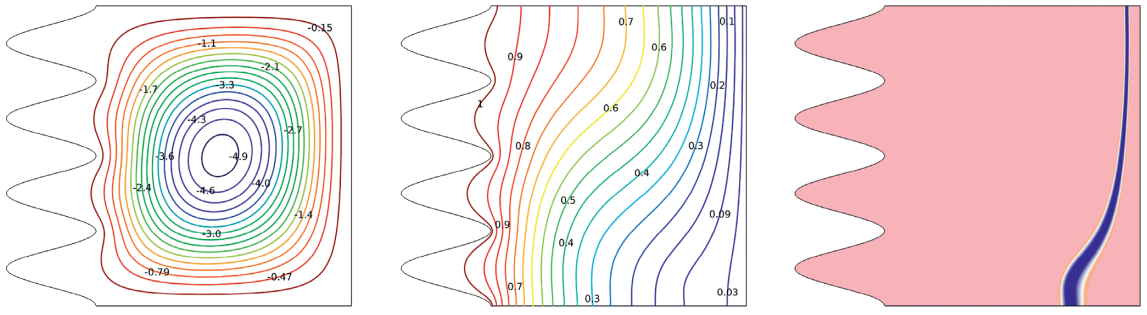

(a)

Figure 6: Continued.

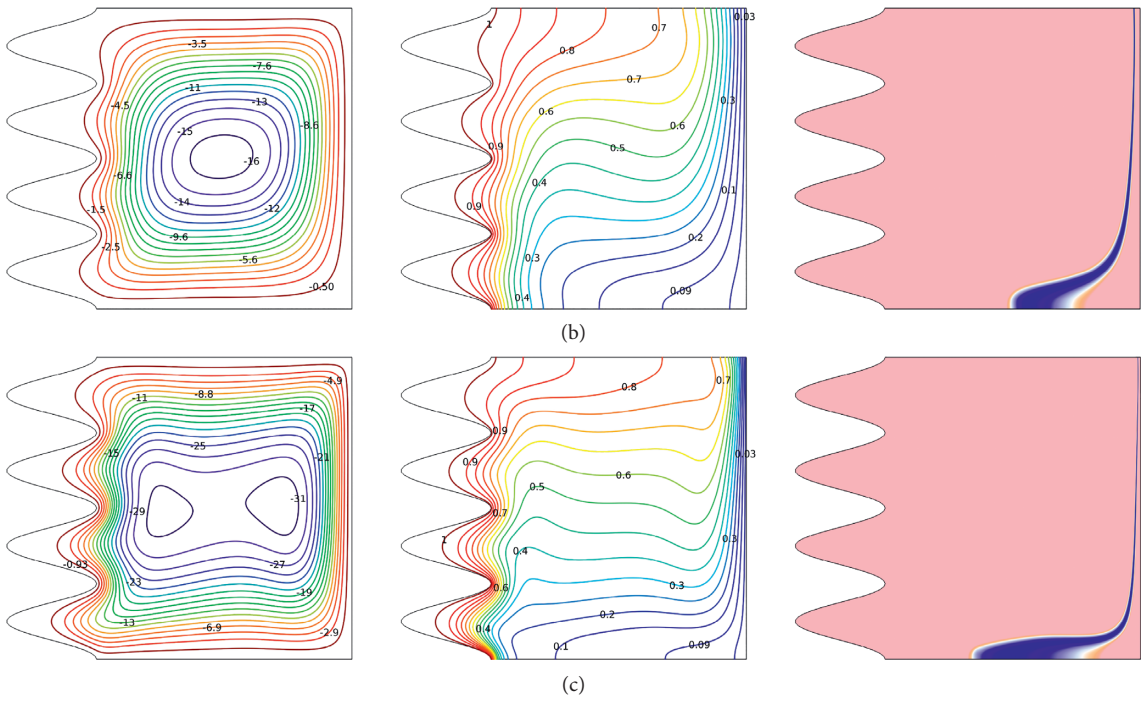

FIGURE 6: Influence of the Rayleigh number on streamlines (left), isotherms (middle), and heat capacity ratio distribution (right) at $\phi = 0.05$, $\theta_f = 0.1$, Ste = 0.2, $A = 0.3$, and $N = 4$. (a) $\mathrm{Ra} = 10^4$. (b) $\mathrm{Ra} = 10^5$. (c) $\mathrm{Ra} = 10^6$.

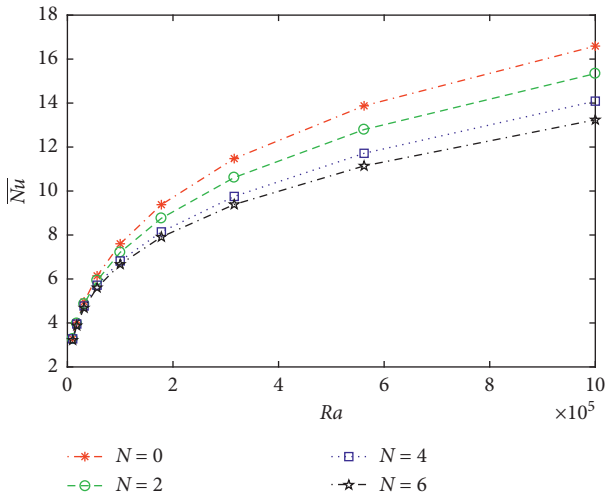

FIGURE 7: Profiles of the average Nusselt number against Rayleigh number for the values of N labelled on the figure at $\phi = 0.05$, $\theta_f = 0.1$, $A = 0.3$, and $N = 4$.

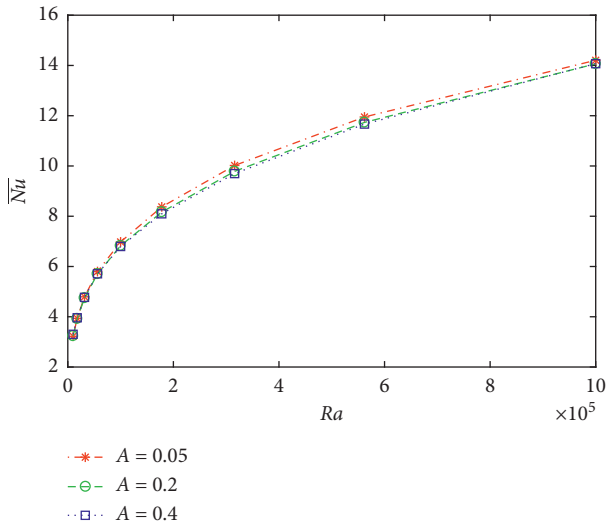

FIGURE 8: Profiles of the average Nusselt number against Rayleigh number for the values of A labelled on the figure at $\phi = 0.05$, $\theta_f = 0.1$, and $N = 4$.

temperature where the phase change area moves closer to isothermal surfaces. The highest heat transfers were achieved about $\theta_f = 0.3$ and $\theta_f = 0.7$. Between these values, there exists the local minimum of the heat transfer, especially at a relative small Stefan number.

Figure 11 exhibits the influence of the heating intensity on the average Nusselt number versus the NEPCM particles volume fraction at $A = 0.3$ and $N = 4$. The enhancement of heat transfer is regardless of the Rayleigh number. The Nusselt number increases by increasing the NEPCM particle volume fraction. The influence of Rayleigh number on the heat transfer rate is different at small and high NEPCM particles volume fraction. At high NEPCM density and small buoyancy force, the core absorbs more heat from the heated surface and then releases fairly large energy when latent heat passes from one state. Hereby, using only 1% of NEPCM particles and with the high Rayleigh number, the heat transfer can be improved more than 12%.

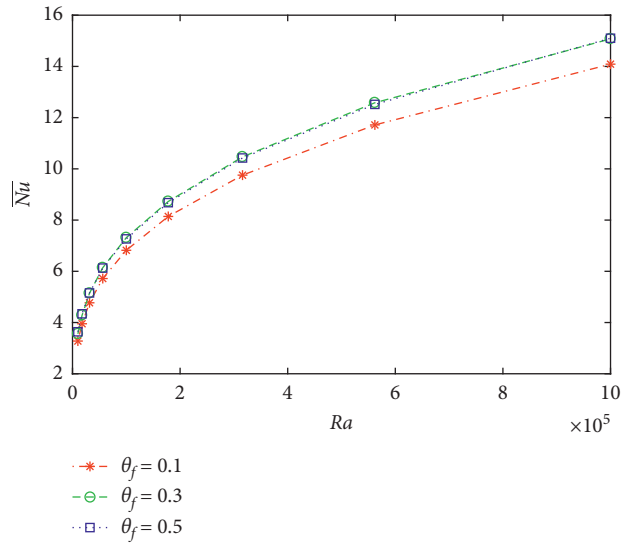

Figure 9: Plots of the average Nusselt number against Rayleigh number for the values of θ_f labelled on the figure at $\phi = 0.05$, Ste = 0.2, $A = 0.3$, and $N = 4$.

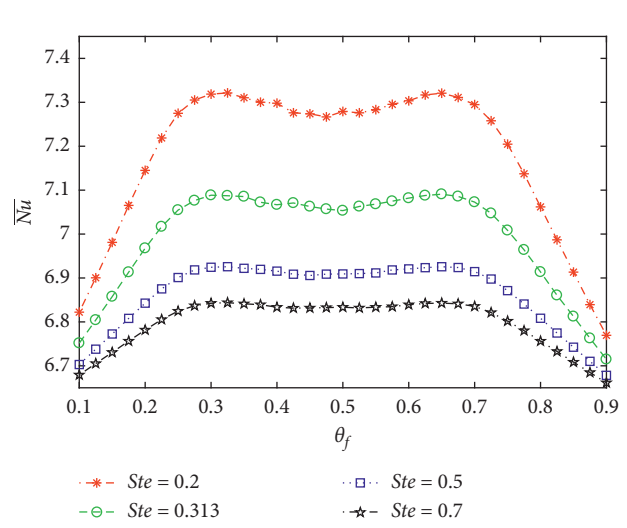

Figure 10: Plots of the average Nusselt number against the fusion temperature for the values of Ste labelled on the figure at $\phi = 0.05$, Ra = 10^5, $A = 0.3$, and $N = 4$.

Figure 12 presents the influence of the concentration on the average Nusselt number versus the undulation number at Ra = 10^6, $A = 0.3$, Ste = 0.2, and $\theta_f = 0.1$. In general, the mean Nusselt number decreases as the undulation number increases at pure water of NEPCM-water. This is due to the fact that the ratio of Nusselt number per unit length of the hot surface decreases as the length of the surface increases. The highest mean Nusselt number can be observed at the lowest undulation number and highest NEPCM particles volume fraction. Finally, the average Nusselt number can be correlated with the undulation number and concentration as well as Rayleigh number as follows:

$$\overline{\mathrm{Nu}} = \frac{(0.21 + 2\phi)}{N^{0.206}} \mathrm{Ra}^{0.29}. \quad (25)$$

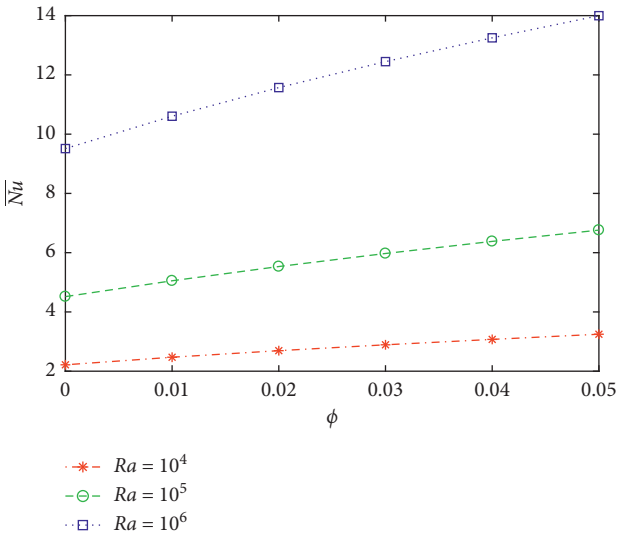

Figure 11: Effects of the heating intensity on the average Nusselt number versus the concentration at $A = 0.3$ and $N = 4$.

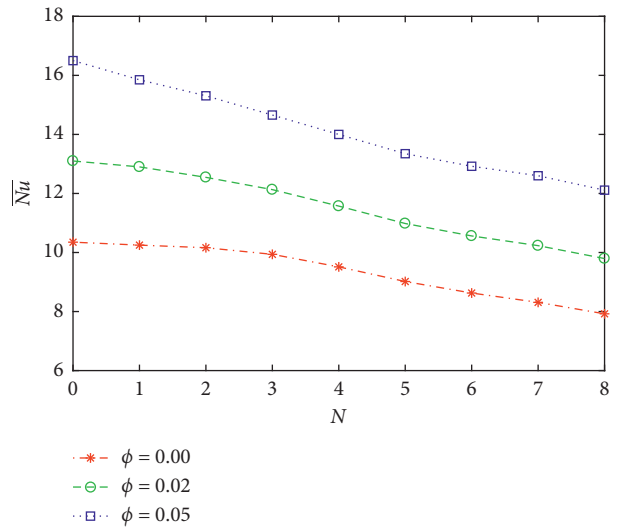

Figure 12: Effects of the undulation number on the average Nusselt number versus the concentration at Ra = 10^6, $A = 0.3$, Ste = 0.2, and $\theta_f = 0.1$.

5. Conclusions

The present study scrutinized the impact of NEPCM, waviness, magnitude of the temperature difference, and the nanoparticle concentration. The equations governing continuity, momentum, and energy inside the wavy cavity are stated in the dimensionless form. The latent heat released and absorbed throughout the phase change by the NEPCM is given in the formulation. The dimensionless forms of the mathematical model are solved numerically by means of the Galerkin FEM. Graphical result of the local and average Nusselt numbers is given and the plots of isotherms, streamlines, and heat capacity ratio are exhibited. The fluids are agitated by the melting, heater size, heating intensity, and

volume fraction parameters. Some important conclusions from the study are given as follows:

(1) The undulation number, fusion temperature, and Rayleigh number are essential aspects in the flow circulation, structure, and its strength

(2) The structure of the isotherm is not affected by the different fusion temperature value, but the area of phase change shifts upwards when the fusion temperatures get higher

(3) Altering the latent heat from the wavy surface temperatures improves the success of the NEPCM in terms of thermal performance enhancement

(4) The global heat transfer can be improved by more than 12% by adding 1% of NEPCM particles volume fraction. However, the heat transfer tends to decrease by applying the wavy surface

Abbreviations

A:	Amplitude of undulations
C_p:	Specific heat capacitance
g:	Accelerating due to gravity
k:	Thermal conductivity
L:	Width and height of cavity
N:	Number of undulations
Nu:	Nusselt number
Pr:	Prandtl number
Ra:	Rayleigh number
S:	Surface area of undulated wall
Ste:	Stefan number
T:	Temperature
u, v:	Velocity components in the x-direction and y-direction
x, y and X, Y:	Space coordinates and dimensionless space coordinates.

Greek Symbols

α:	Effective thermal diffusivity
β:	Thermal expansion coefficient
Θ:	Dimensionless temperature
μ:	Dynamic viscosity
ν:	Kinematic viscosity
ϕ:	Solid volume fraction
ψ and Ψ:	Stream function and dimensionless stream function
ρ:	Fluid density.

Subscripts

b: Hybrid nanofluid
c: Cold
co: Core
f: Fluid
h: Hot
p: NEPCM nanoparticle
sh: Shell.

Data Availability

The data used to support the findings of this study are included in this paper and available without any restrictions.

Conflicts of Interest

The authors declare that there are no conflicts of interest regarding the publication of this research article.

References

[1] S. U. S. Choi, "Enhancing thermal conductivity of fluids with nanoparticles," *American Society of Mechanical Engineers Fluids Engineering Division*, vol. 231, pp. 99–105, 1995.

[2] K. Khanafer, K. Vafai, and M. Lightstone, "Buoyancy-driven heat transfer enhancement in a two-dimensional enclosure utilizing nanofluids," *International Journal of Heat and Mass Transfer*, vol. 46, no. 19, pp. 3639–3653, 2003.

[3] R.-Y. Jou and S.-C. Tzeng, "Numerical research of nature convective heat transfer enhancement filled with nanofluids in rectangular enclosures," *International Communications in Heat and Mass Transfer*, vol. 33, no. 6, pp. 727–736, 2006.

[4] K. S. Hwang, J.-H. Lee, and S. P. Jang, "Buoyancy-driven heat transfer of water-based Al2O3 nanofluids in a rectangular cavity," *International Journal Of Heat And Mass Transfer*, vol. 50, no. 19-20, pp. 4003–4010, 2007.

[5] H. F. Oztop and E. Abu-Nada, "Numerical study of natural convection in partially heated rectangular enclosures filled with nanofluids," *International Journal of Heat and Fluid Flow*, vol. 29, no. 5, pp. 1326–1336, 2008.

[6] M. K. Das and P. Shridhar Ohal, "Natural convection heat transfer augmentation in a partially heated and partially cooled square cavity utilizing nanofluids," *International Journal of Numerical Methods for Heat & Fluid Flow*, vol. 19, no. 3/4, pp. 411–431, 2009.

[7] E. B. Öğüt, "Natural convection of water-based nanofluids in an inclined enclosure with a heat source," *International Journal of Thermal Sciences*, vol. 48, pp. 2063–2073, 2009.

[8] W. Rashmi, A. F. Ismail, M. Khalid, and Y. Faridah, "CFD studies on natural convection heat transfer of Al2O3-water nanofluids," *Heat and Mass Transfer*, vol. 47, no. 10, pp. 1301–1310, 2011.

[9] G. A. Sheikhzadeh, M. Dastmalchi, and H. Khorasanizadeh, "Effects of nanoparticles transport mechanisms on Al2O3-water nanofluid natural convection in a square enclosure," *International Journal of Thermal Sciences*, vol. 66, pp. 51–62, 2013.

[10] S. Y. Motlagh and H. Soltanipour, "Natural convection of Al2O3-water nanofluid in an inclined cavity using Buongiorno's two-phase model," *International Journal of Thermal Sciences*, vol. 111, pp. 310–320, 2017.

[11] E. Abu-Nada and H. F. Oztop, "Numerical analysis of Al_2O_3/water nanofluids natural convection in a wavy walled cavity," *Numerical Heat Transfer, Part A: Applications*, vol. 59, no. 1, pp. 403–419, 2011.

[12] M. Esmaeilpour and M. Abdollahzadeh, "Free convection and entropy generation of nanofluid inside an enclosure with different patterns of vertical wavy walls," *International Journal of Thermal Sciences*, vol. 52, pp. 127–136, 2012.

[13] M. Nikfar and M. Mahmoodi, "Meshless local Petrov-Galerkin analysis of free convection of nanofluid in a cavity with wavy side walls," *Engineering Analysis with Boundary Elements*, vol. 36, no. 3, pp. 433–445, 2012.

[14] M. A. Mansour and M. A. Y. Bakier, "Free convection heat transfer in complex-wavy-wall enclosed cavity filled with nanofluid," *International Communications in Heat and Mass Transfer*, vol. 44, pp. 108–115, 2013.

[15] C.-C. Cho, C.-L. Chen, and C. O.-K. Chen, "Natural convection heat transfer and entropy generation in wavy-wall enclosure containing water-based nanofluid," *International Journal of Heat and Mass Transfer*, vol. 61, pp. 749–758, 2013.

[16] C.-C. Cho, "Heat transfer and entropy generation of natural convection in nanofluid-filled square cavity with partially-heated wavy surface," *International Journal of Heat and Mass Transfer*, vol. 77, pp. 818–827, 2014.

[17] B. Takabi and S. Salehi, "Augmentation of the heat transfer performance of a sinusoidal corrugated enclosure by employing hybrid nanofluid," *Advances in Mechanical Engineering*, vol. 6, p. 147059, 2014.

[18] M. Sheikholeslami, M. Gorji-Bandpy, D. D. Ganji, and S. Soleimani, "MHD natural convection in a nanofluid filled inclined enclosure with sinusoidal wall using CVFEM," *Neural Computing and Applications*, vol. 24, no. 3-4, pp. 873–882, 2014.

[19] M. Sheikholeslami and R. Ellahi, "Electrohydrodynamic nanofluid hydrothermal treatment in an enclosure with sinusoidal upper wall," *Applied Sciences*, vol. 5, no. 3, pp. 294–306, 2015.

[20] W. Tang, M. Hatami, J. Zhou, and D. Jing, "Natural convection heat transfer in a nanofluid-filled cavity with double sinusoidal wavy walls of various phase deviations," *International Journal of Heat and Mass Transfer*, vol. 115, pp. 430–440, 2017.

[21] K. M. Shirvan, R. Ellahi, M. Mamourian, and M. Moghiman, "Effects of wavy surface characteristics on natural convection heat transfer in a cosine corrugated square cavity filled with nanofluid," *International Journal of Heat and Mass Transfer*, vol. 107, pp. 1110–1118, 2017.

[22] M. Sheremet, I. Pop, H. F. Öztop, and N. Abu-Hamdeh, "Natural convection of nanofluid inside a wavy cavity with a non-uniform heating," *International Journal of Numerical Methods for Heat & Fluid Flow*, vol. 27, no. 4, pp. 958–980, 2017.

[23] H. R. Ashorynejad and A. Shahriari, "MHD natural convection of hybrid nanofluid in an open wavy cavity," *Results in Physics*, vol. 9, pp. 440–455, 2018.

[24] I. Hashim, A. I. Alsabery, M. A. Sheremet, and A. J. Chamkha, "Numerical investigation of natural convection of Al_2O_3-water nanofluid in a wavy cavity with conductive inner block using Buongiorno's two-phase model," *Advanced Powder Technology*, vol. 7, 2018.

[25] A. S. Dogonchi, A. J. Chamkha, and D. D. Ganji, "A numerical investigation of magneto-hydrodynamic natural convection of Cu-water nanofluid in a wavy cavity using CVFEM," *Journal of Thermal Analysis and Calorimetry*, vol. 135, no. 4, pp. 2599–2611, 2019.

[26] A. S. Dogonchi, M. Hashemi-Tilehnoee, M. Waqas, S. M. Seyyedi, I. L. Animasaun, and D. D. Ganji, "The influence of different shapes of nanoparticle on Cu-H2O nanofluids in a partially heated irregular wavy enclosure," *Physica A: Statistical Mechanics and Its Applications*, vol. 540, p. 123034, 2020.

[27] S. Kashani, A. A. Ranjbar, M. Abdollahzadeh, and S. Sebti, "Solidification of nano-enhanced phase change material (NEPCM) in a wavy cavity," *Heat and Mass Transfer*, vol. 48, no. 7, pp. 1155–1166, 2012.

[28] S. S. Sebti, M. Mastiani, H. Mirzaei, A. Dadvand, S. Kashani, and S. A. Hosseini, "Numerical study of the melting of nano-enhanced phase change material in a square cavity," *Journal of Zhejiang University SCIENCE A*, vol. 14, no. 5, pp. 307–316, 2013.

[29] C. J. Ho and J. Y. Gao, "An experimental study on melting heat transfer of paraffin dispersed with Al2O3 nanoparticles in a vertical enclosure," *International Journal of Heat and Mass Transfer*, vol. 62, pp. 2–8, 2013.

[30] S. H. Tasnim, R. Hossain, S. Mahmud, and A. Dutta, "Convection effect on the melting process of nano-PCM inside porous enclosure," *International Journal of Heat and Mass Transfer*, vol. 85, pp. 206–220, 2015.

[31] M. Abdollahzadeh and M. Esmaeilpour, "Enhancement of phase change material (PCM) based latent heat storage system with nano fluid and wavy surface," *International Journal of Heat and Mass Transfer*, vol. 80, pp. 376–385, 2015.

[32] N. S. Dhaidan, "Nanostructures assisted melting of phase change materials in various cavities," *Applied Thermal Engineering*, vol. 111, pp. 193–212, 2017.

[33] M. Ghalambaz, A. Doostani, A. J. Chamkha, and M. A. Ismael, "Melting of nanoparticles-enhanced phase-change materials in an enclosure: effect of hybrid nanoparticles," *International Journal of Mechanical Sciences*, vol. 134, pp. 85–97, 2017.

[34] M. Al-Jethelah, S. Humaira Tasnim, S. Mahmud, and A. Dutta, "Melting of nano-PCM in an enclosed space: scale analysis and heatline tracking," *International Journal of Heat and Mass Transfer*, vol. 119, pp. 841–859, 2018.

[35] F. Selimefendigil, H. F. Oztop, and A. J. Chamkha, "Natural convection in a CuO-water nanofluid filled cavity under the effect of an inclined magnetic field and phase change material (PCM) attached to its vertical wall," *Journal of Thermal Analysis and Calorimetry*, vol. 135, no. 2, pp. 1577–1594, 2019.

[36] N. S. Bondareva, B. Buonomo, O. Manca, and M. A. Sheremet, "Heat transfer performance of the finned nano-enhanced phase change material system under the inclination influence," *International Journal of Heat and Mass Transfer*, vol. 135, pp. 1063–1072, 2019.

[37] W. Su, J. Darkwa, and G. Kokogiannakis, "Review of solid-liquid phase change materials and their encapsulation technologies," *Renewable and Sustainable Energy Reviews*, vol. 48, pp. 373–391, 2015.

[38] G. Fang, H. Li, F. Yang, X. Liu, and S. Wu, "Preparation and characterization of nano-encapsulated n-tetradecane as phase change material for thermal energy storage," *Chemical Engineering Journal*, vol. 153, no. 1-3, pp. 217–221, 2009.

[39] A. Jamekhorshid, S. M. Sadrameli, and M. Farid, "A review of microencapsulation methods of phase change materials (PCMs) as a thermal energy storage (TES) medium," *Renewable and Sustainable Energy Reviews*, vol. 31, pp. 531–542, 2014.

[40] E. M. Shchukina, M. Graham, Z. Zheng, and D. G. Shchukin, "Nanoencapsulation of phase change materials for advanced thermal energy storage systems," *Chemical Society Reviews*, vol. 47, no. 11, pp. 4156–4175, 2018.

[41] H. Nazir, M. Batool, F. J. Bolivar Osorio et al., "Recent developments in phase change materials for energy storage applications: a review," *International Journal of Heat and Mass Transfer*, vol. 129, pp. 491–523, 2019.

[42] M. Ghalambaz, A. J. Chamkha, and D. Wen, "Natural convective flow and heat transfer of nano-encapsulated phase change materials (NEPCMs) in a cavity," *International Journal of Heat and Mass Transfer*, vol. 138, pp. 738–749, 2019.

[43] A. Hajjar, S. A. M. Mehryan, and M. Ghalambaz, "Time periodic natural convection heat transfer in a nano-encapsulated phase-change suspension," *International Journal of Mechanical Sciences*, vol. 166, p. 105243, 2020.

[44] S. Barlak, O. N. Sara, A. Karaipekli, and S. Yapıcı, "Thermal conductivity and viscosity of nanofluids having nano-encapsulated phase change material," *Nanoscale and Microscale Thermophysical Engineering*, vol. 20, no. 2, pp. 85–96, 2016.

[45] J. C Maxwell-Garnett, "Colours in metal glasses and in metallic films," *Philosophical Transactions of the Royal Society A*, vol. 203, pp. 385–420, 1904.

[46] L. Chai, R. Shaukat, L. Wang, and H. S. Wang, "A review on heat transfer and hydrodynamic characteristics of nano/microencapsulated phase change slurry (N/MPCS) in mini/microchannel heat sinks," *Applied Thermal Engineering*, vol. 135, pp. 334–349, 2018.

[47] L. Adjlout, O. Imine, A. Azzi, and M. Belkadi, "Laminar natural convection in an inclined cavity with a wavy wall," *International Journal of Heat and Mass Transfer*, vol. 45, no. 10, pp. 2141–2152, 2002.